

F. Galbusera · A. Fantigrossi · M.T. Raimondi  
M. Sassi · M. Fornari · R. Assietti

## Biomechanics of the C5-C6 spinal unit before and after placement of a disc prosthesis

Received: 15 September 2005 / Accepted: 27 December 2005  
© Springer-Verlag 2006

**Abstract** The study consists of a biomechanical comparison between the intact C5–C6 spinal segment and the same segment implanted with the Bryan™ artificial disc prosthesis (Medtronic Ltd., Memphis, TN, USA), by the use of the finite element (FE) method. Our target is the prediction of the influence of prosthesis placement on the resulting mechanics of the C5–C6 spine unit. A FE model of the intact C5–C6 segment was built, employing realistic models of the vertebrae, disc and ligaments. Simulations were conducted imposing a compression preload combined to a flexion/extension moment, a pure lateral bending moment and a pure torsion moment, and the calculated results were compared to data from literature. The model was then modified to include the Bryan™ cervical disc prosthesis, and the simulations were repeated. The location of the instantaneous center of rotation (ICR) of C5 with respect to C6 throughout flexion/extension was calculated in both models. In general, the moment–rotation curves obtained from the disc prosthesis-implanted model were comparable to the curves obtained from the intact model, except for a slightly greater stiffness induced by the artificial disc. The position of the calculated ICRs was rather stable throughout flexion–extension and was generally confined to a small area, qualitatively matching the corresponding physiological region, in both models. These results imply that the Bryan™ disc prosthesis allows to correctly reproduce a physiological flexion/extension at the implanted level. The results of this study have quantified aspects that may

assist in optimizing cervical disc replacement primarily from a biomechanical point of view.

### 1 Introduction

This paper presents a biomechanical study of the C5–C6 functional spine unit after the placement of a disc prosthesis. Recently, disc arthroplasty has been adopted by many surgeons. For a number of years, cervical spinal diseases have been treated primarily with anterior cervical decompression and fusion procedures, which provide a good rate of success and early recovery of the patient (Hilibrand et al. 2004). Cervical plating has further improved the success rate, reducing morbidity and allowing earlier return to employment. However, clinical studies showed that fusion is associated with a decreased range of motion and leads to accelerated adjacent segment degeneration (Anderson et al. 2004). Spinal arthroplasty, which provides motion preservation of the implanted functional spine unit, could reasonably slow down or eliminate adjacent segment degeneration (Anderson et al. 2004; Anderson and Rouleau 2004; DiAngelo et al. 2003; Goffin et al. 2003). It is realistic to presume that the maintenance of motion at a spinal unit may result in improved load transfer and reduced stress on the adjacent intervertebral discs and posterior elements (Smith et al. 2004). Thus, surgeons are becoming increasingly interested in performing arthroplasty instead of fusion, even if its long-term clinical benefit with respect to arthrodesis remains to be demonstrated.

A number of commercial and experimental cervical disc prostheses are now available. Unfortunately, testing procedures and methods to predict the biomechanical adequacy of these devices have not yet been established. Furthermore, the intermediate and long-term clinical results are not documented in the literature, except in a few cases involving a small number of patients (Goffin et al. 2003), even if many preliminary clinical reports are available (Duggal et al. 2004; Anderson et al. 2004). The biomechanics of the implanted cervical spine appears even less investigated. Some *in vitro* experimental studies have been carried out, using cadaver

F. Galbusera (✉) · A. Fantigrossi · M.T. Raimondi  
Laboratory of Biological Structure Mechanics,  
Department of Bioengineering, Politecnico di Milano,  
Piazza Leonardo da Vinci, 32  
20133 Milan, Italy  
Tel.: +39-02-66214939  
Fax: +39-02-66214939  
E-mail: fabio.galbusera@biomed.polimi.it

R. Assietti  
Ospedale Fatebenefratelli e Oftalmico, Milan, Italy

M. Sassi · M. Fornari  
Istituto Ortopedico Galeazzi, Milan, Italy

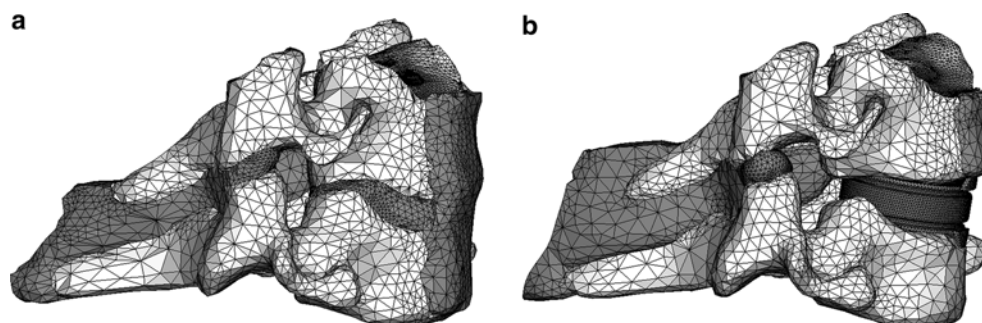


**Fig. 1** Finite element model of the intact C5–C6 spinal unit (a) (177,857 elements, 102,609 degrees of freedom) and of the same unit implanted with the Bryan disc prosthesis (b) (176,727 elements, 101,958 degrees of freedom)

specimens implanted with a disc prosthesis, where the results are compared to analogous experiments performed on the intact spine. DiAngelo et al. (2003) investigated the stiffness of a cervical spine implanted with a Prestige<sup>TM</sup> (Medtronic Ltd., Memphis, TN, USA) disc prosthesis, and compared it with the stiffness of an intact and an anterior-plated cervical spine. McAfee et al. (2003) compared the range of motion of an intact cervical spine with that of a fused spine and that of a spine implanted with the PCM<sup>TM</sup> prosthesis (Cervitech Inc., Rockaway, NJ, USA). Only a few authors have examined the biomechanics of the cervical spine implanted with the Bryan<sup>TM</sup> disc prosthesis (Medtronic Ltd.), using experimental methods to determine the wear resistance of the device (Anderson et al. 2004) and using elaboration of bioimages to study the spine alignment after prosthesis placement (Johnson et al. 2004; Pickett et al. 2004). In all these studies, the very complex 3D motion of the cervical spine is simplified to a basic bidimensional flexion/extension in the sagittal plane. A comprehensive study of the 3D biomechanics of a cervical functional spine unit implanted with a cervical disc prosthesis remains currently unavailable in the literature.

A technique commonly employed to investigate the spinal biomechanics is the construction of mathematical models and their solution using numerical methods, e.g. the finite element (FE) method. These methods have been demonstrated to be very useful in research related to biomechanics, since they allow the quantification of variables not directly measurable in experimental studies, such as local stresses, and they facilitate determination of the influence of single parameters on the resulting biomechanics of complex structures. The literature includes many studies describing FE models of the intact cervical spine (Yoganandan et al. 1996; Maurel et al. 1997; Teo and Ng 2001; Goel and Clausen 1998). Some authors focus on cervical fusion procedures (Teo et al. 2004; Pitzen et al. 2002), but, to our knowledge, computational studies predicting the biomechanics of the spine implanted with a cervical disc prosthesis have not yet been performed.

The purpose of this study is the determination of the biomechanics of a cervical spinal unit implanted with a commercially available disc prosthesis (Bryan<sup>TM</sup>, Medtronic Ltd., Memphis, TN, USA), which will be simply referred to as Bryan hereafter, as compared to the biomechanics of the unimplanted segment. To this purpose, 3D FE models of

both the intact C5–C6 unit and of the same unit implanted with the prosthesis were set up and comparative simulations were run in various loading configurations. The model of the intact C5–C6 segment was validated using consolidated biomechanical data on cervical flexion/extension. The result of the simulations are discussed in relation to the clinical setting in which these devices are employed.

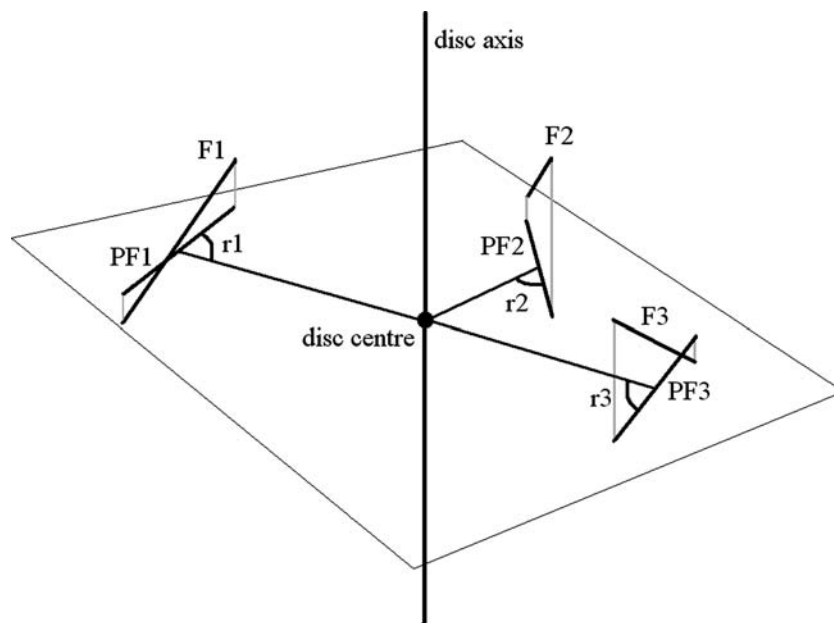
## 2 Materials and methods

Firstly, a 3D FE model of the intact C5–C6 functional spine unit was built (Fig. 1a). This model was aimed to represent a healthy segment, without any degenerative sign. The geometry of the two vertebrae was reconstructed from computer tomography (CT) scans taken from the Visible Human Dataset, a collection of radiographic images and photos of sections of the whole human body made available by the American National Institute of Health. A commercial software (Amira, TGS, San Diego, CA, USA) was used to transform the planar CT scans into solid models of the vertebrae considered. The intervertebral disc was represented as a continuum structure occupying the intervertebral space and laterally limited to the middle of the uncinat processes. The anterior and posterior disc heights assumed were 5.5 and 3.5 mm respectively, which correspond to the mean values found in the literature for a healthy cervical intervertebral disc (Maurel et al. 1997). The structure was subdivided into an inner volume representing the nucleus pulposus and an external layer representing the annulus fibrosus. Ligaments modeled were the anterior longitudinal ligament (ALL), the posterior longitudinal ligament (PLL), the flaval ligament (FL) and the interspinous ligament (ISL). All ligaments were modeled as continua. The joint capsules (JC) were modeled as solid entities including the space between the superior tip of the cephalad facet to the inferior tip of the caudal facet (Yoganandan et al. 2000; Kumaresan et al. 1998).

The geometrical entities (nucleus pulposus, annulus fibrosus, ligaments, vertebrae, which include the body, transverse processes, pedicles, laminae and spinous process) were then discretized into linear tetrahedral elements. A finer discretization was adopted in the regions near the intervertebral disc and the facet joints. Thin triangular shell elements, with

**Table 1** Mechanical properties and total number of elements of the components of the FE models

	E (MPa)	$\nu$	Number of elements (intact model)	Number of elements (Bryan model)
Cancellous bone	100	0.3	83,599	96,288
Cortical bone	12,000	0.3	22,432	25,398
ALL	28	0.45	5,053	2,051
PLL	23	0.45	4,891	1,679
FL	3.5	0.45	5,353	6,183
ISL	5	0.45	4,852	5,128
JC	5	0.45	6,338	6,544
Disc nucleus	0.1	0.499	15,919	NA
Disc annulus – matrix	2.5	0.45	25,567	NA
Disc annulus – fibers	500	0.35	3,853	NA
Titanium	110,000	0.3	NA	18,058
Polyurethane	25	0.45	NA	15,398

**Fig. 2** Definition of the orientation of three representative fibers  $F1$ ,  $F2$  and  $F3$  with respect to the radial direction. Orientation ( $r1$ ,  $r2$ ,  $r3$  angles) is defined as the value of the sharpest angle between the projection of the fiber on the axial plane (PF1, PF2, PF3) and the line that connects the center of the disc and the mid-point of the projection of the fiber

the thickness of 1 mm, were adopted to model the cortical shell and the endplates. The constitutive model assigned to all materials, except for the ligaments and the JC, was the linear isotropic elastic. Ligaments were simulated using tension-only tetrahedral solid elements. To avoid possible numerical instabilities caused by this type of element in solving the nonlinear FE equations, each element of the ligaments was overlaid with a correspondent linear elastic element with a small Young modulus (0.1 MPa), thus creating a negligible artificial stiffness in compression. The JC were modeled using the same elements of the ligaments. Contact with no friction was defined between the articular surfaces of the facet joints. Material properties assigned to each entity are reported in Table 1 (Yoganandan et al. 2000, 2001; Maurel et al. 1997).

In order to better simulate the nonlinear behavior of the intervertebral disc, truss elements were introduced in the annulus fibrosus, as done in previous studies (Maurel et al. 1997), to model the collagen fibers. The truss elements were

initially relaxed and only allowed to transmit tension forces. All the truss elements were defined with equal elastic properties (Table 1) (Lu et al. 1998). The average volume fraction assumed for the truss elements, with respect to the volume of the annulus fibrosus, was 0.20. Since the collagen fibers are believed to be less important in determining the disc mechanics in the lateral region, if compared to the anterior and posterior regions (Maurel et al. 1997), fewer truss elements were introduced near the uncinat processes. A C++ code was developed to automatically build a set of truss elements, with specified cardinality, that best fits some chosen parameters: mean length of the fibers, mean orientation of the fibers with respect to the axial plane, mean orientation with respect to the radial direction (Fig. 2). Optimal values were then chosen for each parameter: 3 mm for the mean fiber length,  $30^\circ$  for the orientation with respect to the axial plane,  $90^\circ$  for the orientation with respect to the radial direction. Considering all the defined requirements, the code builds an

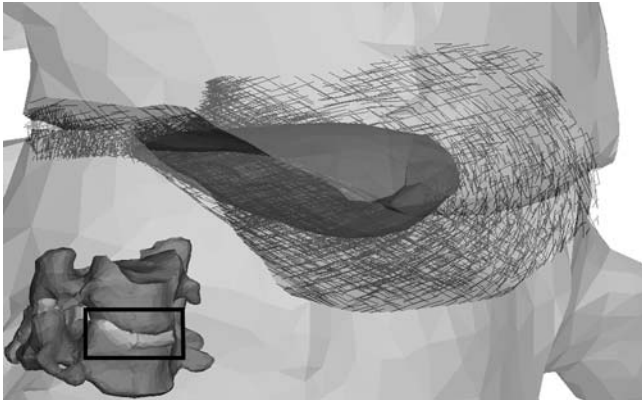


**Fig. 3** Model of the intervertebral disc including the nucleus pulposus and the truss elements used to represent collagen fibers. The solid elements of the annulus fibrosus matrix are not here displayed

optimized set of truss elements by selecting their endpoints between the nodes constituting the annulus fibrosus (Fig. 3).

The FE model was run to evaluate the moment–rotation response under an axial compressive preload of 73.6 N combined with a moment of 1.8 Nm in sagittal flexion or extension (Goel and Clausen 1998; Teo and Ng 2001), a pure lateral flexion moment of 1 Nm and a pure torsion moment of 1 Nm. The computations were conducted using the commercial FE code ABAQUS 6.4 (ABAQUS Inc., Providence, RI, USA), taking into account geometric nonlinearity. Four static simulations were carried out, in flexion, in extension, in lateral bending and in axial rotation. The lower endplate of C6 was fixed in all the simulations and load steps. The simulations of sagittal flexion and extension included two load steps: a first step in which the axial compressive preload of 73.6 N was applied, and a second step for the addition of the specific moment of 1.8 Nm in flexion or extension. The axial preload was applied as a distributed load acting on the free element faces pertaining to the upper endplate of C5. To impose the moments, a set of concentrated forces acting on several nodes on the upper endplate of C5 was defined. The value of each force was determined in order to make the force system result in a moment of the prescribed value and satisfy the translational equilibrium. For each analysis, a moment–rotation response curve was built, considering as rotation values the principal rotation angles of C5 around the moment axis. The curves obtained with the FE model were compared to the experimental and computational data from previous studies (Teo and Ng 2001), to assess the validity of the model. A stiffness coefficient  $K$  ( $\text{Nm}/^\circ$ ) was calculated for each moment–rotation plot as the slope of the linear regression line passing through the origin of the load–displacement plane.

The FE model of the C5–C6 intact functional spinal unit was then modified to simulate the biomechanics of the segment after implantation of the Bryan cervical disc prosthesis. An adequate prosthesis size (diameter 18 mm) was chosen analyzing the CT scans of the spinal unit. A 3D solid model of the Bryan prosthesis was built and included into the FE model of the intact segment (Fig. 1b). The Bryan prosthesis

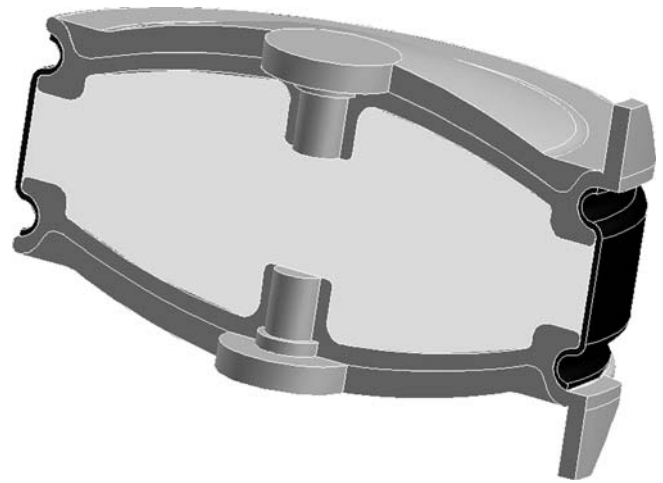


**Fig. 4** Section view of the Bryan disc prosthesis 3D model; the internal nucleus (*white*), the titanium shells (*gray*) and the flexible membrane (*black*) are identifiable

contains a low-friction, wear-resistant polyurethane nucleus, which is located between, and articulates with, shaped titanium plates that include convex porous ingrowth surfaces, to allow bony fixation to the adjacent vertebral endplates. A flexible membrane surrounds the interior articulating shell surfaces, to separate the internal structures of the device from the external in vivo environment and to contain a lubricant. The FE model of the prosthesis included four components: the upper and the lower shells, the flexible external membrane and the internal nucleus (Fig. 4). The internal nucleus was considered to be attached to the shells; thus sliding at the interfaces was assumed to be impossible in this model. All the components were meshed into linear tetrahedral elements, and modeled as linear isotropic elastic materials. The elastic properties assigned to the components are reported in Table 1. To properly locate the prosthesis within the FE model, the intervertebral disc was firstly removed, and the distance between the vertebrae was increased by 1 mm to simulate distraction. A socket conformal to the shape of the shells was then created into the C5 and C6 vertebral bodies. The ALL portion facing the intervertebral space was removed to simulate the surgical procedure. Although the removal of the corresponding PLL portion is not strictly required by the surgical technique, it is performed by many surgeons and is thus included in the present model. The vertebral cortical shell was removed on the endplates, to simulate the milling stage of the surgical technique. The interaction between the prosthesis shells and the vertebral socket was modeled as a tie constraint, which means that each node on one surface is constrained to have the same displacements as the point on the corresponding surface to which it is closest. Four simulations were conducted, with the same boundary conditions of the intact case. Moment–rotation curves in sagittal flexion and extension, lateral bending and axial rotation were obtained and compared to the corresponding curves from the intact model. The stiffness coefficient,  $K$ , was calculated for each simulation, as for the intact model.

A parameter taken into account in the evaluation of the biomechanical performance of the Bryan prosthesis, other than the stiffness  $K$  described above, was the mean position and the stability of the instantaneous center of rotation (ICR) of C5 with respect to C6, during flexion and extension. Assuming that the ICR could be considered stable and the deformations of the vertebral bodies could be neglected during each increment of the second step of the analyses, the contours of the vertebrae for each couple of consecutive increments were imported into the general-purpose image manipulation application GIMP (open-source, <http://www.gimp.org>) and processed to obtain the location of the ICR. The determination of the ICR was achieved using the Euler method (Penning 1988). Landmarks were arbitrarily placed in a different anatomical position of the C5 vertebral contour. The landmarks were again determined on a consecutive incremental contour, and then connected to the one previously determined using connection lines (Fig. 5). The process was repeated for the following contours. The mid-perpendiculars on the connection lines intersected at the ICR. To quantify the position of the graphically determined ICR, a polar frame of reference was introduced, with the origin in the center of the upper C6 endplate and with the polar axis aligned to the same endplate; thus the ICR position could be described by a vector  $\mathbf{v}$  having radius  $\rho$  and azimuth  $\theta$  (Fig. 6). The positions of the ICRs were determined for each couple of increments of the flexion and extension simulations, for both the intact model and the Bryan model.

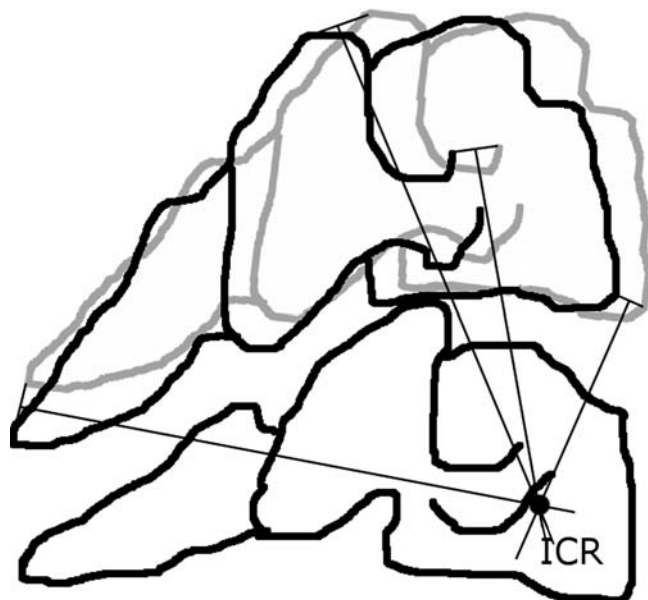


**Fig. 5** Schematic representation of the Euler method for the localization of the instantaneous center of rotation (ICR). Landmarks are arbitrarily placed in a different anatomical position of the C5 vertebral contour. The landmarks are again determined on a consecutive incremental contour, and then connected to the one previously determined using connection lines. The process is repeated for the following contours. The mid-perpendiculars on the connection lines intersect at the ICR

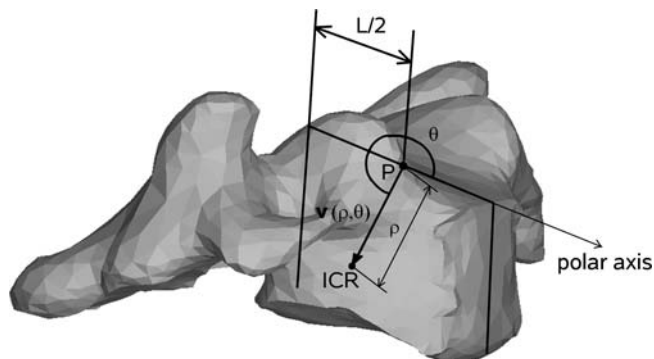


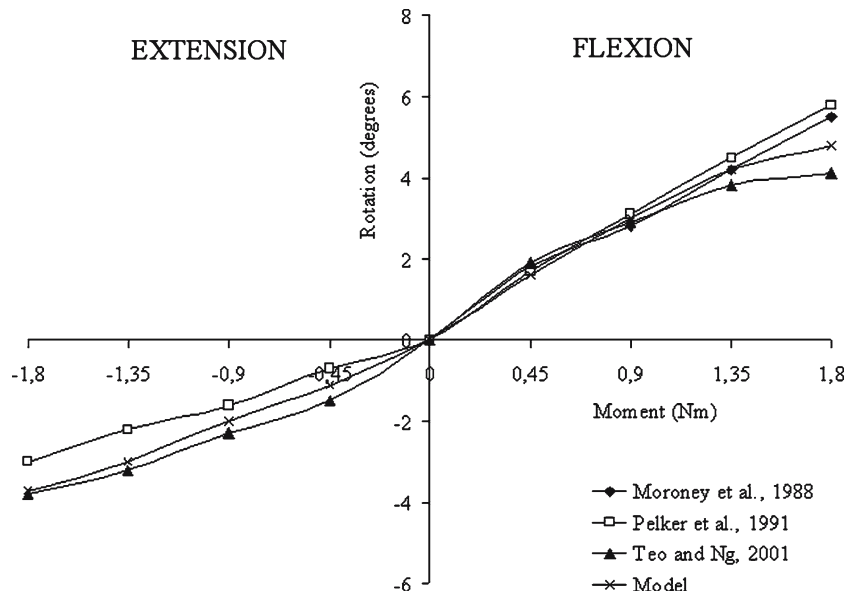
**Fig. 6** Method adopted to quantify the position of the graphically determined ICR. A polar frame of reference with the origin positioned in the center of the upper C6 endplate is defined, for the determination of the ICR polar coordinates  $\rho$  and  $\theta$ . The center of the C6 endplate is defined at a distance  $L/2$  from the posterior margin of the vertebral body

### 3 Results

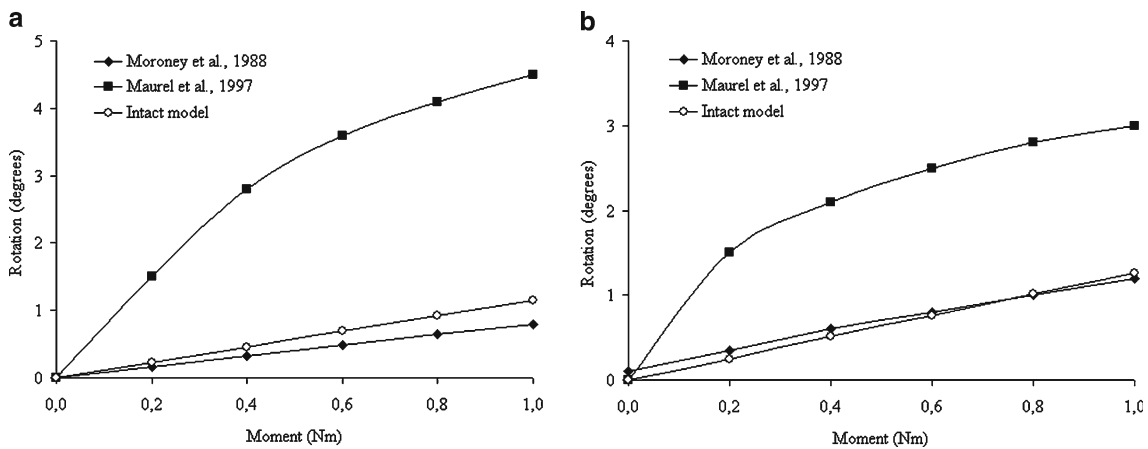
Figure 7 shows the moment–rotation curve of the C5–C6 intact model in sagittal flexion–extension, plotted together with experimental and computational data from the literature (Teo and Ng 2001). All the comparison curves were obtained with the boundary and loading conditions adopted in this study. The qualitative agreement of our results with the previous studies is evident. The curve shows a slightly greater mean stiffness in extension than in flexion, coherently with other authors (Pelker et al. 1991). The nonlinear stiffening at higher values of the sagittal moment, predicted by other authors (Teo and Ng 2001), is confirmed here. The calculated moment–rotation curves in lateral bending and axial rotation are reported in Fig. 8, together with the literature data obtained in the same loading and boundary conditions. Again, the results presented in this study qualitatively agree with previous data.

Figure 9 reports the moment–rotation curves in sagittal flexion–extension calculated with the intact and the Bryan models. The curves are similar in extension, while the Bryan model exhibits a higher stiffness in flexion to that of the intact model. This asymmetry is due not only to the mechanics of the prosthesis itself, but also to the ligaments removal during the surgical procedures, which have a significant stabilizing role during flexion–extension of the intact segment. Again, the implanted spinal unit exhibits a stiffening for increasing values of the moment magnitude, apparently less marked if compared to the stiffening calculated for the intact model.

Figure 10 shows the moment–rotation curves in lateral bending and axial rotation obtained with the intact and the Bryan models. In both cases, the curves obtained with the Bryan model exhibit a slope comparable, even if slightly higher, to those computed with the intact model. A summary of the results is reported in Table 2, which contains the stiffness of the intact and the implanted segment calculated for the four load cases considered (flexion, extension, lateral bending, axial rotation). Coherently with the previous results, the segment implanted with the Bryan prosthesis exhibits a



**Fig. 7** Moment–rotation diagram for the intact model in flexion–extension, compared with data from the literature obtained with the same calculated loading conditions



**Fig. 8** Moment–rotation diagram for the intact model in lateral bending (a) and axial rotation (b), compared with the data from literature

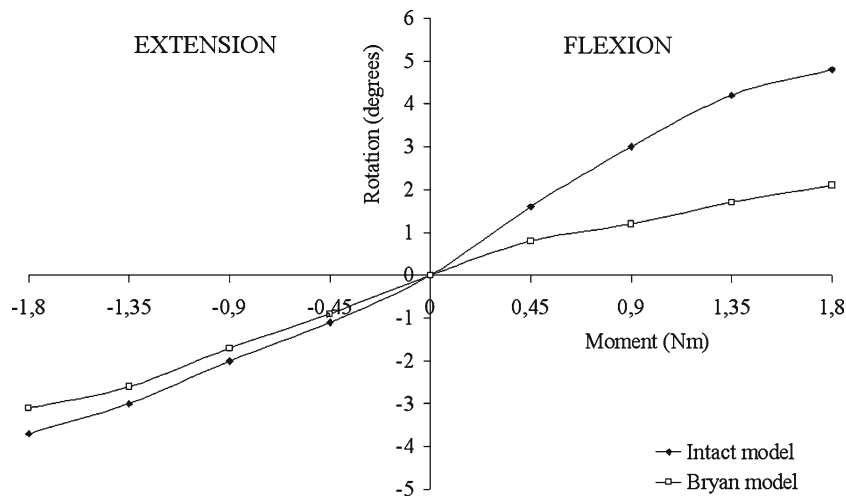


**Fig. 9** Moment–rotation curves for the intact model and the Bryan model in flexion–extension

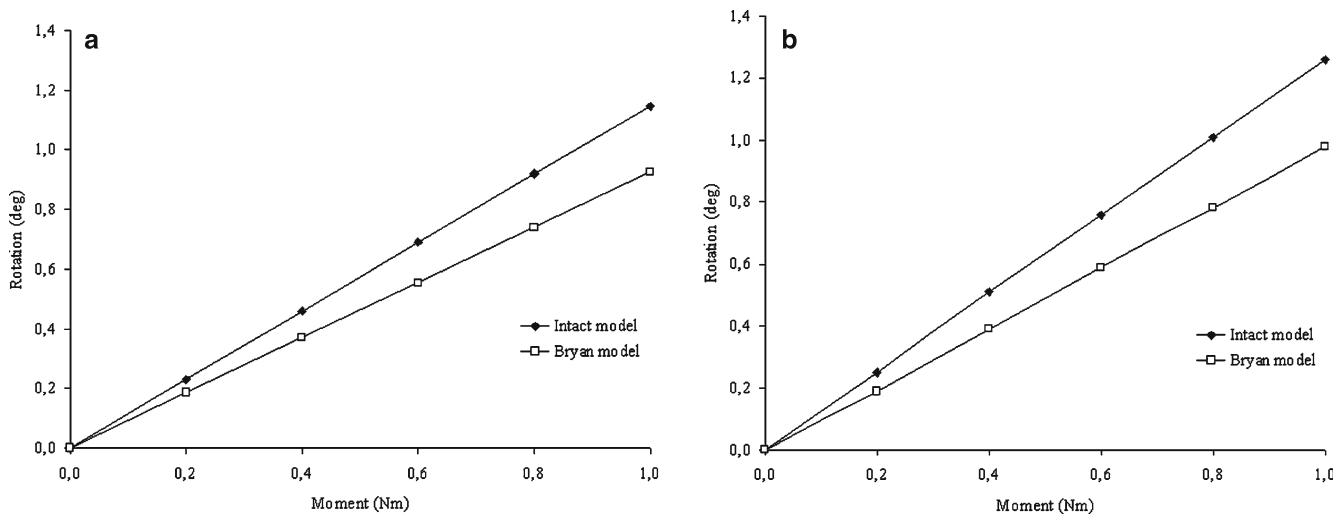


**Fig. 10** Moment–rotation curves for the intact model and the Bryan model in lateral bending (a) and axial rotation (b)

**Table 2** Stiffness coefficients  $K(\text{Nm}/^\circ)$  calculated at the considered loading conditions

	Intact model [ $\text{K}(\text{Nm}/^\circ)$ ]	Bryan model [ $\text{K}(\text{Nm}/^\circ)$ ]
Flexion	0.4	0.9
Extension	0.5	0.6
Lateral bending	0.9	1.1
Axial rotation	0.8	1

stiffness increase if compared to the intact segment, for all loading conditions. However, this increase does not seem to be enough to sensitively reduce the segment motion under physiological loading.

Figure 11 shows the areas containing all the ICRs calculated at the load increments considered mapped on a section of C6, for the intact (Fig. 11a) and the implanted (Fig. 11b) models. The areas are quite similar and both reside in the region below the center of the upper endplate of C6, consistently with several observations conducted in previous studies (Penning 1988; Amevo et al. 1991; Bogduk and Mercer 2000). Table 3 reports the calculated location of the ICR in polar coordinates, obtained from the intact and the Bryan models, for each load increment. For the intact case, the mean radius (distance between the ICR and the mid-point of the C6 upper endplate) is 3.3 mm, with a standard deviation of 0.24. For the Bryan model, the calculated mean radius is 3.4 mm and its standard deviation is 1.34. The low value of the standard deviation for the intact case is coherent with experimental and cineradiographic studies that show how the ICR position is stable during flexion–extension (Bogduk and Mercer 2000). The standard deviation value obtained with the Bryan model testifies a less stable position of the ICR during flexion–extension if compared to the intact case; however, the area in which the ICR is located appears reasonably circumscribed.

## 4 Discussion

This paper presents two detailed 3D FE models of the intact C5–C6 functional spine unit and of the same segment after insertion of a cervical disc prosthesis. Of the many FE models of the lower cervical spine available in the literature, the earlier models were not geometrically detailed. Some described the vertebral bodies with simplified geometrical entities and discarded important features like the posterior elements and the uncinat processes (Hosey and Liu 1982). More recent studies included detailed representations of the vertebrae, while discarding material and geometrical nonlinearity (Yoganandan et al. 1996), except for few papers considering them (Teo and Ng 2001). Commonly reported results are load–displacement curves in compression, sagittal flexion and extension (Yoganandan et al. 1996; Teo and Ng 2001). Teo and Ng (2001) built a nonlinear FE model of the C5–C6 functional spine unit, and studied it in compression and sagittal flexion–extension, by comparing their results to previous studies (Moroney et al. 1988; Pelker et al. 1991). These data were used to validate the intact model in the current study; thus, the loading and constraint conditions imposed were identical to those from the cited papers. The stiffness coefficients in lateral flexion and axial rotation, calculated with the intact model, appear very similar to the data reported by Maurel et al. (1997), who simulated 12 different functional units imposing a moment of 2 Nm superimposed to a compressive preload of 6 N. These authors found stiffness coefficients of  $0.9 \text{ Nm}/^\circ$  in lateral flexion and  $0.85 \text{ Nm}/^\circ$  in axial rotation, while in the present study the correspondent results were 0.9 and  $0.8 \text{ Nm}/^\circ$ . The literature includes very few studies presenting moment–rotation results in lateral bending and axial rotation. The calculated results qualitatively agree with these data, in particular with the experimental study carried out by Moroney et al. (1988). For these loading conditions, the moment–rotation curves appear linear. This result is reasonably due to the relatively low value of

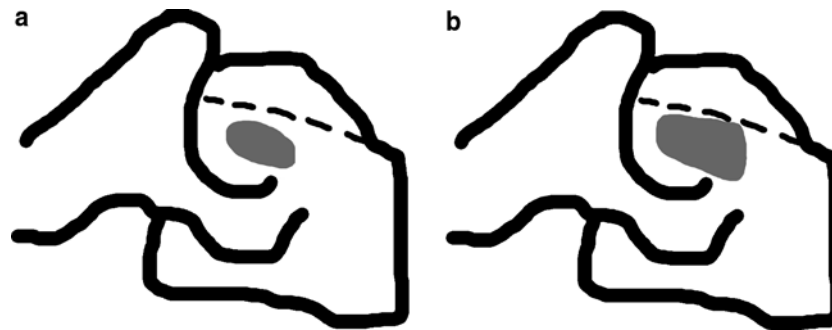


**Fig. 11** Approximate areas containing the ICRs in flexion–extension for the intact (a) and the Bryan (b) models

**Table 3** Calculated locations of the ICRs during the various load increments in polar coordinates

Intact model			Bryan model		
Moment (Nm)	$\rho$ (mm)	$\theta$ (°)	Moment (Nm)	$\rho$ (mm)	$\theta$ (°)
–1.8 to –1.35	3.8	320	–1.8 to –1.35	4.0	310
–1.35 to –0.9	3.5	300	–1.35 to –0.9	4.0	300
–0.9 to –0.45	3.5	280	–0.9 to –0.45	3.2	270
–0.45 to 0	3.2	260	–0.45 to 0	1.5	260
0 to 0.45	3.0	250	0 to 0.45	1.0	250
0.45 to 0.9	3.2	250	0.45 to 0.9	3.5	250
0.9 to 1.35	3.3	250	0.9 to 1.35	4.5	240
1.35 to 1.8	3.3	250	1.35 to 1.8	4.2	240
Mean	3.3		Mean	3.4	
Standard Deviation	0.24		Standard Deviation	1.34	

the imposed loads; a nonlinear behavior could be expected for higher loads. In general, considering the accord between the results obtained with the FE model and the information available in the literature, the model showed to be a valuable prediction tool.

The presented models, as every mathematical model of complex phenomena, include some simplifications necessary to build a manageable model of the real structure. Living tissues have extremely complex mechanics which are often not yet comprehensively investigated. For these structures, a lot of modeling strategies, more or less sophisticated, were described in the previous studies. The intervertebral disc, for example, has been included in the FE studies with several approaches: almost-incompressible solid elements (Goel and Clausen 1998) or fluid elements for the nucleus pulposus (Yoganandan et al. 1996); anisotropic solid, fiber-reinforced composite or more complex continuum elements for the annulus fibrosus (Yin and Elliott 2005). In the present work, the intervertebral disc is modeled using classical approaches which, despite their simplicity, are capable of capturing the segment biomechanics with good accuracy. A fiber-reinforced composite, which has been used in many literature studies with reliable results (Yoganandan et al. 2001), is adopted for the annulus fibrosus. The nucleus pulposus is modeled employing almost-incompressible solid elements (Goel and Clausen 1998). The constitutive model adopted for the ligaments, which has been employed in previous studies (Yoganandan et al. 1996; Maurel et al. 1997), represents a more severe limitation of the present work, but gives reason-

ably accurate results if the loads are not very high (Yoganandan et al. 2001).

Patients subjected to cervical arthroplasty have often a degenerated spine, determined by the remodeling of bony structures, intervertebral discs and facet joints; thus a simulation of a degenerative state could be of practical interest. However, the spinal degeneration process is likely to be related with several factors of a different nature (mechanical, biological, biochemical) and thus impossible to simulate with a purely mechanical model without making strong assumptions. A possible modeling strategy is considering a specific degenerative state and neglecting the temporal evolution, for example reducing disc height and modifying the mechanical properties of the nucleus pulposus (Rohlmann et al. 2005). However, degeneration is usually highly variable from patient to patient; thus the definition of a standard degenerative state to be used as basis for the calculation is not straightforward. In this study the authors chose to investigate the biomechanics of arthroplasty on a healthy segment, targeting the work on the investigation of the biomechanical effect of prosthesis and the surgical procedure themselves instead of their influence on a specific degenerative state.

To our knowledge, biomechanical evaluations of the Bryan cervical prosthesis directly comparable to the present study are not currently available in the literature. Duggal et al. (2004) presented a biomechanical study based on the radiographs of an implanted patient. In this study, the authors performed a motion analysis in flexion–extension using radiographs on 22 patients implanted with a Bryan prosthesis on a single level. The authors measured the overall cervical spinal motion, and stated that it is not significantly altered. Sagittal rotation was found not to change significantly at any level after surgery. The same prediction can be formulated from our FE results, since the calculated moment–rotation curves are similar for the intact model and the Bryan model.

Many literature papers investigated the locations and measuring of the ICRs in flexion–extension for intact cervical segments (Penning 1988; Amevo et al. 1991; Bogduk and Mercer 2000). However, equivalent studies concerning the cervical spine after arthroplasty are currently unavailable. As stated above, the calculated area in which the ICRs are located appears to be rather similar to the correspondent area on the intact segment. This result, together with the findings on the stiffness of the implanted segment, brings us to the conclusion

that a cervical segment implanted with the Bryan prosthesis has a mechanical behavior comparable to a physiological segment. Thus, placement of the prosthesis has a limited effect on the biomechanics of the cervical spine, coherently with results from the literature (Duggal et al. 2004), suggesting a more favorable outcome on the preservation of adjacent discs with respect to fusion.

The clinical results of the Bryan prosthesis were published by many authors (Duggal et al. 2004; Anderson et al. 2004; Goffin et al. 2003). Even if based on short follow-up times due to the relatively recent introduction of the prosthesis, the clinical outcome seems to be satisfactory, not inferior to fusion procedures. However, the convenience of implanting a disc prosthesis in terms of the risk/benefits ratio with respect to fusion remains to be proved. Clinical studies demonstrated that the motion elimination at one level, consequent to fusion, leads to hypermobility and increased stresses at adjacent levels, thus increasing the rate of disc degeneration (Hilibrand et al. 2004). The supposed advantage of cervical arthroplasty versus fusion is reduction of the risk of early disc degeneration at adjacent levels, resulting from the preservation of the mobility of the implanted level. In other words, if the implanted segment can be considered biomechanically equivalent to an intact segment, placement of the prosthesis should not generate mechanical alterations which could induce early degeneration of the adjacent discs. Based on this assumption, an effective way to predict the long-term outcome of cervical arthroplasty is the biomechanical evaluation of the implanted spinal unit. Clearly, only clinical studies based on long follow-ups can demonstrate the convenience of the risk/benefit ratio of cervical arthroplasty and ensure the absence of other possible adverse outcomes.

**Acknowledgements** Funding by Medtronic Ltd. is gratefully acknowledged.

## References

- Amevo B, Worth D, Bogduk N (1991) Instantaneous axes of rotation of the typical cervical motion segments: a study in normal volunteers. *Clin Biomech* 6:111–117
- Anderson PA, Rouleau JP (2004) Intervertebral disc arthroplasty. *Spine* 29:2779–2786
- Anderson PA, Sasso RC, Rouleau JP et al. (2004) The Bryan cervical disc: wear properties and early clinical results. *Spine J* 4(6 Suppl):303S–309S
- Bogduk N, Mercer S (2000) Biomechanics of the cervical spine. I: Normal kinematics. *Clin Biomech* 15(9):633–648
- DiAngelo DJ, Roberston JT, Metcalf NH et al. (2003) Biomechanical testing of an artificial cervical joint and an anterior cervical plate. *J Spinal Disord Tech* 16(4):314–323
- Duggal N, Pickett GE, Mitsis DK et al. (2004) Early clinical and biomechanical results following cervical arthroplasty. *Neurosurg Focus* 17(3):E9
- Goel VK, Clausen JD (1998) Prediction of load sharing among spinal components of a C5-C6 motion segment using the finite element approach. *Spine* 23(6):684–691
- Goffin J, Van Calenbergh F, van Loon J et al. (2003) Intermediate follow-up after treatment of degenerative disc disease with the Bryan cervical disc prosthesis: single-level and bi-level. *Spine* 28(24):2673–2678
- Hilibrand AS, Robbins M (2004) Adjacent segment degeneration and adjacent segment disease: the consequences of spinal fusion? *Spine J* 4:190S–194S
- Hosey RR, Liu YK (1982) A homeomorphic finite element model of the human head and neck. In: Gallagher RH, Simon BR, Johnson PC, Gross JF (eds) *Finite elements in biomechanics*. Wiley, New York, pp 379–401
- Johnson JP, Laurysen C, Cambron HO et al. (2004) Sagittal alignment and the Bryan cervical artificial disc. *Neurosurg Focus* 17(6):E14
- Kumaresan S, Yoganandan N, Pintar FA (1998) Finite element modeling approaches of human cervical spine facet joint capsule. *J Biomech* 31(4):371–376
- Lu YM, Hutton WC, Gharpuray VM (1998) The effect of fluid loss on the viscoelastic behavior of the lumbar intervertebral disc in compression. *J Biomech Eng* 120(1):48–54
- Maurel N, Lavaste F, Skalli W (1997) A three-dimensional parameterised finite element model of the lower cervical spine. Study of the influence of the posterior articular facets. *J Biomech* 30(9):921–931
- McAfee PC, Cunningham B, Dmitriev A et al. (2003) Cervical disc replacement-porous coated motion prosthesis: a comparative biomechanical analysis showing the key role of the posterior longitudinal ligament. *Spine* 28(20):S176–S185
- Moroney SP, Schultz AB, Miller JAA, Andersson GBJ (1988) Load-displacement properties of lower cervical spine motion segments. *J Biomech* 21:767–779
- Pelker RR, Duranceau JS, Panjabi MM (1991) Cervical spine stabilization. A three-dimensional, biomechanical evaluation of rotational stability, strength, and failure mechanisms. *Spine* 16(2):117–122
- Penning L (1988) Differences in anatomy, motion, development and aging of the upper and lower cervical disk segments. *Clin Biomech* 3:37–47
- Pickett GE, Mitsis DK, Sekhon LH et al. (2004) Effects of a cervical disc prosthesis on segmental and cervical spine alignment. *Neurosurg Focus* 17(3):E5
- Pitzen TR, Matthis D, Barbier DD et al. (2002) Initial stability of cervical spine fixation: predictive value of a finite element model. Technical note. *J Neurosurg Spine* 97(1):128–134
- Rohlmann A, Zander T, Schmidt H, Wilke HJ, Bergmann G (2005) Analysis of the influence of disc degeneration on the mechanical behaviour of a lumbar motion segment using the finite element method. *J Biomech* (in press)
- Smith HE, Wimberley DW, Vaccaro AR (2004) Cervical arthroplasty: material properties. *Neurosurg Focus* 17(3):E3
- Teo EC, Ng HW (2001) Evaluation of the role of ligaments, facets and disc nucleus in lower cervical spine under compression and sagittal moments using finite element method. *Med Eng Phys* 23:155–164
- Teo EC, Yang K, Fuss FK et al. (2004) Effects of cervical cages on load distribution of cancellous core: a finite element analysis. *J Spinal Disord Tech* 17(3):226–231
- Yin L, Elliott DM (2005) A homogenization model of the annulus fibrosus. *J Biomech* 38(8):1674–1684
- Yoganandan N, Kumaresan SC, Liming Voo et al. (1996) Finite element modeling of the C4-C6 cervical spine unit. *Med Eng Phys* 18(7):569–574
- Yoganandan N, Kumaresan SC, Pintar FA (2000) Geometric and mechanical properties of human cervical spine ligaments. *J Biomech Eng* 122(6):623–629
- Yoganandan N, Kumaresan SC, Pintar FA (2001) Biomechanics of the cervical spine Part 2. Cervical spine soft tissue responses and biomechanical modeling. *Clin Biomech* 16:1–27